Nanoelectromagnetic materials

4

Peter Burke[1] *and Duška Kleut*[2]
[1]University of California, Irvine, Samueli School of Engineering, Irvine, CA, United States; [2]Vinča Institute of Nuclear Sciences-National Institute of the Republic of Serbia, University of Belgrade, Department of Radiation Chemistry and Physics, Belgrade, Serbia

4.1 Introduction

We are currently witnessing a remarkable progress in electromagnetic (EM) functional materials, with a special focus on nanoscale and low-dimensional materials. These advancements enable significant strides in high-tech applications, uncovering new physical effects and properties while fostering innovation in fields like EM wave absorption, shielding, sensing, imaging, optics, and photovoltaics. The integration of material and technology sciences around nano- and micromaterials is a crucial driver for developing cutting-edge EM functional devices [1].

The increasing global demand for sustainable energy has steered researchers toward the advancement of smart hierarchical two-dimensional (2D) materials and their composites. Among these, 2D materials such as transition metal carbides/nitrides (MXenes), layered double hydroxides (LDHs), and graphene oxide (GO) hold immense potential for energy storage applications. This potential arises from their exceptional attributes, including unique morphologies, impressive thermomechanical properties, and remarkable electrical, electronic, EM, and magnetic characteristics [2].

Nano-EM materials can be made of composites including one-dimensional (1D) and 2D basic building blocks. In this chapter, we start from the basic interactions of electromagnetic waves (EMWs) with reduced-dimensional systems, discuss the empirical performance of composites made of these systems, and conclude with models relating the two, with perspectives for the future at the end.

4.2 Basic electromagnetic properties of 1D and 2D materials

Nanowires, nanotubes, and nanorods represent 1D, linear materials a 1000 times thinner than a human hair. They brought a groundbreaking innovation to nanomaterial applications in computing, photonics, energy, and biomedical technologies [3].

Key advancements in 1D material research include the development of the "vapor–liquid–solid process" by Dr. R. S. Wagner in the 1960s, which laid the foundation for nanowire research [4]. This process, often using gold as a catalyst, inspired subsequent innovations, enabling the growth of nanowires with precise control over their dimensions and properties.

Electromagnetic Interference Shielding Materials. https://doi.org/10.1016/B978-0-443-36630-7.00006-5

In the 1990s and beyond, researchers expanded the study of semiconductor nanowires to include various materials like oxides, III–V compounds, and elemental semiconductors. Advances like nanoparticle-catalyzed growth techniques and in situ observations of nanowire formation further propelled the field, allowing for the predictable synthesis of single-crystal nanowires [5].

In the last 2 decades, nanotubes, especially carbon nanotubes, and nanowires have transformed into a dynamic interdisciplinary field, enabling the creation of advanced devices in electronics, photonics, biomedicine, and energy storage [6–8]. Notably, researchers have used nanowires to build components like p–n junctions, transistors, and three-dimensional (3D) circuits, unlocking new possibilities for future technologies. This ongoing research continues to expand the frontiers of material science and device engineering [9–13].

Since its isolation in 2004, graphene has sparked extensive research in 2D materials, leading to the establishment of an entire subdiscipline in physical sciences. Graphene, as a 2D material composed of sp^2 hybridized carbon atoms forming carbon sheets, has been extensively used in electronics due to its excellent electrical, mechanical, and thermal properties, as well as its low density, making it a lightweight material. Studies have shown that pristine graphene does not exhibit good microwave absorption (MA) properties because of its high conductivity, leading to impedance mismatching. Therefore, reduced graphene or graphene with dopants is being used as a promising candidate for microwave (MW)-absorbing materials. The distinctive 2D structure provides immense flexibility for customization and functionalization, allowing control over features like layer count, defects, morphology, moiré patterns, and strain [9,14–17].

2D materials exhibit unique physical and chemical characteristics that make them highly advantageous for applications in MA and electromagnetic interference (EMI) shielding. These materials demonstrate effective shielding and absorbing responses to EMI [10]. This chapter will present the research progress in the synthesis, EM performance, and MW shielding/absorbing mechanisms of 2D materials, the introduction of heteroatoms, the construction of unique structures, and the development of 2D composite materials [18–20].

Reduced-dimensional materials interact with EMs in a fundamentally different way than bulk materials, depending on the frequency and dimensionality. For example, in reduced-dimensional materials, the quantum capacitance becomes comparable to the electrostatic capacitance, as shown below in Fig. 4.1.

In addition, kinetic inductance dominates magnetic inductance by up to four orders of magnitude in low electronic density materials [27]. We review next how these quantum and reduced dimensionality effects result in different regimes of operation depending on the frequency and dimensionality.

4.3 One-dimensional (1D) materials

4.3.1 High frequency

At high frequencies compared to the scattering frequency (typically around a few hundred GHz), the imaginary part of the response function dominates any real absorption.

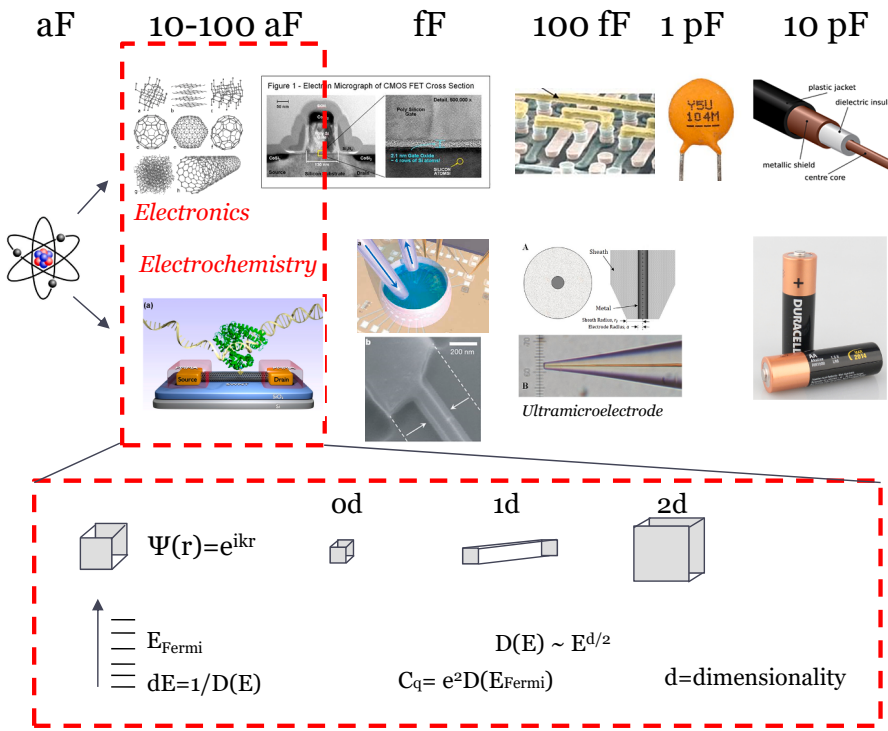

Figure 4.1 Capacitance of reduced-dimensional systems. The finite spacing between energy levels and its relationship to the dimensionality of the system is shown on the bottom. On the top are shown various systems, their associated dimensions, and capacitances. Capacitance of reduced-dimensional systems.
Modified from E. Stern, F. James, Klemic, A. David, Routenberg, N. Pauline, Wyrembak, B. Daniel, Turner-Evans, D. Andrew, Hamilton, A. David LaVan, M. Tarek, Fahmy, M.A. Reed, Label-free immunodetection with CMOS-compatible semiconducting nanowires, Nature 445 (7127) (2007) 519–522; G. Hou, Z. Lu, N. Vianessa, W. Zhizhen, S. Mark, Review of recent advances in carbon nanotube biosensors based on field-effect transistors, Nano Life 6 (3n04) (2016) 1642006; E.L. Muetterties, T.N. Rhodin, B. Elliot, C.F. Brucker, W.R. Pretzer, "Clusters and surfaces", Chemical Reviews 79 (2) (1979) 91–137; Intel; S. Freire, M. Víctor, "Fabrication and characterization of macroscopic graphene layers on metallic substrates." (2014); Tigelaar, Howard, and Howard Tigelaar. "The Incredible Shrinking IC: Part 3 BEOL Aluminum Alloy Single and Multilevel Metal." How Transistor Area Shrank by 1 Million Fold (2020) 227–252

This gives rise to a quantum transmission line type behavior: The characteristic impedance is on the order of the resistance quantum e^2/h (25 kΩ). This is in contrast to a classical transmission line where the electric capacitance and magnetic inductance give rise to a characteristic impedance of order the impedance of free space ~377 Ω $\left(\sqrt{\frac{\mu_0}{\varepsilon_0}}\right)$. In addition, the wave velocity on the line is much slower than the speed of

light, typically about 100 times slower, and of order the Fermi velocity. Because the frequency at which this occurs is in the relatively nascent THz frequency band, it is not widely applicable to most RF and MW technology in broad use today. This was discussed in detail in the THz band in Ref. [27]. Extension to the optical, where electron-hole pair generation takes a significant role, has been presented in Ref. [28].

4.3.2 Low frequency

At low frequencies, the EM properties of 1D materials are dominated by the scattering loss, and become dominantly resistive materials. For example, the resistance per unit length in 1D carbon nanotubes is about 6 kΩ/μ at room temperature [29]. This is much larger than the characteristic impedance of free space, so an individual 1D conductor typically does not interact strongly with free space plane waves, even though their length can be of the same order of magnitude. However, this establishes a quantitative baseline for composite materials based on ensembles of 1D materials, discussed in detail below.

4.4 Two-dimensional (2D) materials

4.4.1 High frequency (THz to optical)

In 2D materials, Geim et al. [30] were the first to show experimentally and theoretically that the real part of the sheet impedance of graphene in the optical is the resistance quantum e^2/h for a single layer. This was later shown by Javey and Yablonovich, both experimentally and theoretically, to be a universal property of 2D materials [11]. This result deserves some discussion. First, this is the real part of the impedance, and is involved in dissipative (absorptive) interaction with EMWs. Second, remarkably, the effect is universal for all 2D quantum systems and independent of the quality (impurities and scattering time) of 2D materials. This is a remarkable property. The mathematical reason for this is the p dot A coupling in the Hamiltonian. However, at least this author does not have a simple, intuitive explanation at this time. Third, it is independent of frequency, within the range of validity of the assumptions (much larger than the inverse scattering time in frequency, and much smaller than the Fermi energy). Fourth, the property also causes very weak interaction of EMWs, due to the inherent impedance mismatch between free space 377 Ω and quantum e^2/h 25 kΩ. In optics, the absorption coefficient is then 2%. It is given fine-structure constant ($\alpha = e^2/\hbar c$) and is approximately 2.3% ($\pi\alpha$). This means for meaningful interaction with radiation, it must be combined in parallel to multilayer 2D materials or composites, discussed below. Fifth, it leads to an amazing practical property: The ability to see a single atomic layer thin material: The 2.3% absorption of graphene on a glass slide can be resolved with the naked eye: A human can see quantum mechanics (e^2/h) and a single atomic layer material and experience both first hand without any instruments at all.

The imaginary part is dominated by plasmonic effects, which is a rephrasing of the RF language of kinetic inductance. This gives rise to guided wave-type behavior observed in a myriad of experimental configurations [31–34], such as standing waves and resonators of various geometries. Since the electronic density can be tuned with a dc voltage (adjusting the Fermi energy), many of these cavity resonances can be tuned electrically.

4.4.2 Low frequency (Sub 100 GHz)

Below the scattering frequency, we and others have shown that the sheet impedance is dominantly a resistive impedance, with negligible effect from the imaginary part [35]. In particular, we have shown that it is possible to get perfect impedance matching to free space in a 2D material, see below. The basic concept is as follows: Below the scattering frequency (1/tau), the impedance is dominantly resistive, i.e., real, and equal to the dc resistance. This is set by the density of electrons and the scattering time. However, most as-produced graphene has a fairly large sheet resistance (several kΩ), so it interacts only weakly with electromagnetic radiation (EMR). In addition, getting large-area graphene (comparable in size laterally to the RF-GHz-THz wavelength) also requires additional focus and attention to growth conditions. For example, we and others have shown it is possible to grow single-crystal graphene over cm areas by carefully engineering of the catalyst and growth rate in a chemical vapor deposition (CVD) reactor [36]. Using this result and careful fabrication techniques, we have shown it is possible to reduce the sheet resistance to be on the order of the characteristic impedance of free space, giving perfect absorption properties. The details are shown in Fig. 4.2 below. Furthermore, unlike most nanomaterial absorption demonstrations, this is broadband, from DC to 1 THz. This incredible result shows almost perfect absorption of MW radiation across a broad frequency range from dc to several hundred GHz by a material only one atom thick. The prospects for exploiting this in EM shielding and wave manipulation are exciting and discussed in more detail later in this chapter.

4.5 Toward a unifying general theory of nanoelectromagnetics

Although most of the pieces are in place of the puzzle, we are not quite at a comprehensive, quantitative theory and experiment of EM properties of reduced-dimensional quantum materials over the entire spectrum. We can start to put some of the pieces together in a possible future unifying theory by summarizing what is known and what is unknown. Fig. 4.3 attempts to create such a picture. From a technology perspective, in particular, we note 2D materials are tunable to be a perfect impedance match to free space as a single layer, in the GHz-THz range. This provides a very important basic technological building block for a large class of EM materials from composites of 2D ingredients, the subject of the next part of this chapter

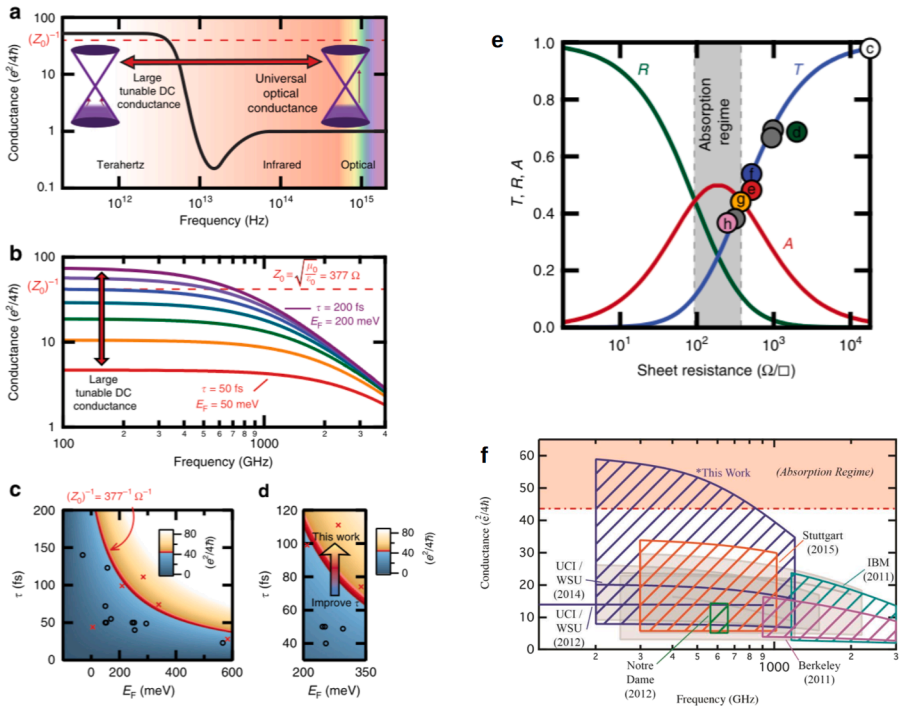

Figure 4.2 Electrical properties of graphene (a) A qualitative trend of frequency-dependent AC conductance for monolayer graphene with normalization to $e^2/4h$. The optical frequency range exhibits a universal value of 1, while in the THz range, the AC conductance can be orders of magnitude higher. (b) Theoretical trend of THz AC conductance for monolayer graphene plotted with a linear variation of the E_F and τ. Graphene samples can cross the free space conductance value, $(Z_0)^{-1}$, within the THz regime. (c) Device design plot showing the graphene sheet conductance (at 100 GHz) in units of $(e^2/4h)$ for changes in E_F and τ. The $(Z_0)^{-1}$ threshold is set as red on the color scale. Previous graphene THz device parameters are plotted as circles, whereas those from this work are denoted as x's. By decreasing the electron scattering in our devices to increase τ, the $(Z_0)^{-1}$ threshold can be crossed into the absorption-dominating regime. (e) The measured transmittance peak values (at ~655 GHz) are plotted as a function of sheet resistance. The theoretical transmittance, absorbance, and reflectance values calculated from the half-wave resonance case for a device on a substrate are plotted as solid lines. The transmittance value becomes less than the absorbance value at sheet resistance values < 377 Ω/□, marking the beginning of the absorption regime. (f) Conductance versus frequency range of other graphene devices in the literature. Hashed regions indicate frequency domain systems, while the transparent gray regions show time-domain measurements. Electrical properties of graphene.

Modified from P. Pham, Z. Weidong, V. Nhi, L. Jinfeng, Z. Weiwei, S. Dominic, R.B. Elliott, P. J. Burke, "Broadband impedance match to two-dimensional materials in the terahertz domain", Nature Communications 8 (1) (2017) 2233.

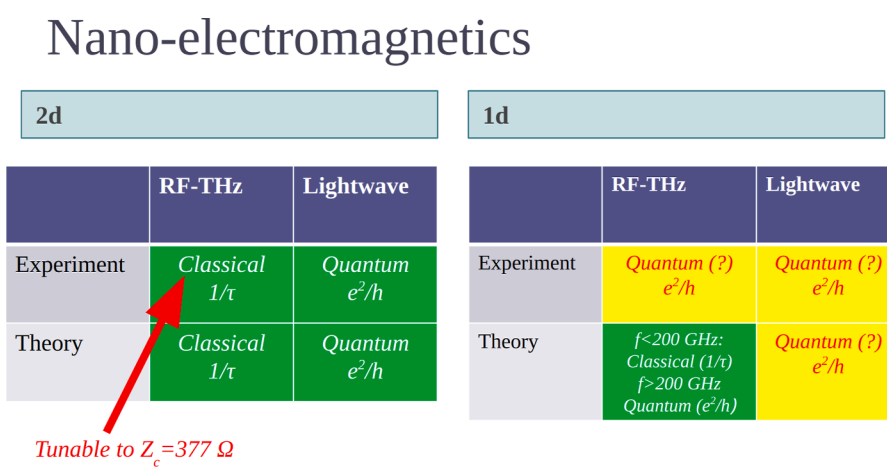

Figure 4.3 Summary of state-of-the-art theoretical and experimental understanding of electromagnetics of reduced-dimensional systems. Summary of state-of-the-art theoretical and experimental understanding of electromagnetics of reduced-dimensional systems.

4.6 Methods of making composites from 1D and 2D materials

This overview covers the synthesis methods, EM properties, and MW shielding/absorbing mechanisms of nano-EM and composite materials as well as their possible applications (sensors, actuators, energy harvesters, storage devices, and solar cells) [37–39].

Conductive carbon materials, including carbon black, graphite, carbon fibers, carbon nanotubes (CNTs), and graphene, have been extensively explored for fabricating EMI shielding materials. Among these, CNTs and graphene stand out for their exceptional ability to create high-performance EMI shielding materials with superior shielding effectiveness (SE) and flexibility [19].

CNTs, as 1D carbon materials, are among the most commonly used in EMI shielding. They are often combined with polymer matrices to create films, which are easy to produce and well-suited for large-scale applications while maintaining excellent EMI shielding capabilities. By blending CNTs with polymers, a uniform dispersion is achieved, and the CNT content is optimized until the composite becomes electrically conductive. Typically, the EMI SE of these composites is directly linked to their electrical conductivity.

Graphene, MXenes, and transition metal dichalcogenides (TMDs), along with their derivatives, are some of the most promising 2D and layered materials for effective EMI shielding [40–42]. Their layered structure enhances multiple reflection and scattering of EMWs among their nanosheets. Combining graphene, MXene, and TMD materials with various conducting polymers, metals, and metal oxides allows for the tuning of EM field absorption. To achieve optimal EMI shielding, materials

need to possess a suitable combination of electrical conductivity, dielectric properties, and magnetic characteristics. By incorporating conductive polymers and metal oxides into graphene and MXene materials, it is possible to alter their magnetic and dielectric properties while maintaining their electrical conductivity, ultimately enhancing EMI shielding performance. Among various metal oxides, Fe_3O_4 is increasingly utilized in EMI shielding materials due to its affordability, high absorption capacity, strong spin polarization, and magnetic behavior.

Innovative work in the creation of advanced multifunctional films has paved the way for next-generation materials suitable for high-end applications [39]. These films have spurred global research efforts and are widely considered for enhancing the physical, chemical, and mechanical properties of metals, ceramics, and composites. Several simple and cost-effective manufacturing methods, such as layer-by-layer processes, solution casting, vacuum filtration, and melt blending, have been instrumental in bringing 2D materials to the commercial scale.

Currently, 3D printing technologies, including extrusion-based, photopolymerization-based, and powder-based methods, are enabling the creation of complex hierarchical structures with outstanding properties [43]. These technologies are particularly effective for developing graphene and graphene/polymer composites. This section focuses on the recent advancements in various versatile synthesis techniques for 2D composite materials and their hybrids.

4.6.1 Graphene materials

Graphene and its related materials have been identified as exceptional candidates for, among other things, EMI shielding due to their high electrical conductivity, robust mechanical strength, large surface area, low density, and increased porosity [44]. These materials, in various forms, have demonstrated impressive EMI SE. For instance, 3D graphene aerogel with a microporous structure showcased a maximum EMI SE of 43.29 dB, attributed to its high electrical conductivity (181 S/m) and mechanical strength [45]. Additionally, thin films and free-standing films of graphene have been synthesized to create multiple interfaces that efficiently reflect and scatter EMWs. The presence of oxygen functionalities in some graphene derivatives enhances MW attenuation by inducing dipolar polarization. Graphene materials are often used as conductive fillers in polymer matrices for graphene-polymer composites. They also serve as matrices for conductive nanoparticles in EMI shielding applications [46].

In addition to these advanced graphene materials, other graphene-related materials, such as graphene/quartz fabric, rGO foam, and rGO nanoplatelet foam, have also been utilized for EMI shielding applications. To further enhance shielding performance, graphene materials have been integrated with metal oxides, MXenes, and LDHs [47].

4.6.2 Graphene – metal composites

Metals, known for their ability to transmit, reflect, and absorb EMI, are excellent conductors, while plastics and rubbers are nonconductive and transparent to EMI.

Researchers have employed various methods to synthesize shielding composites combining graphene with metals and other materials, achieving notable SE [48]. Methods such as hydrothermal, solvothermal, and scalable techniques have produced composites tested up to the Ku-band frequency range. Notably, hydrothermal and solvothermal methods achieved reflection losses of −55.02 dB and −59.23 dB, respectively, while the scalable method attained an SE of 52.4 dB in the X-band. Alternating deposition in the THF band yielded an SE of 60.95 dB. Techniques like in situ growth, facile synthetic routes, and electrophoretic deposition have also demonstrated high SE in different frequency ranges. The materials' properties and preparation methods play crucial roles in determining the composites' structure and shielding performance.

For example, a reduced graphene oxide (rGO) and silver (Ag) nanowire network exhibited low sheet resistance, improved reflection loss, and significant EM absorption attenuation in the X-band region [49]. The fabrication process involved electrodeposition and pulsed laser irradiation, where defects in the graphene sheets generated dielectric polarization, and functional groups on the graphene surface acted as dipolar polarization centers. The interfacial polarization arose from the resistivity difference between Ag nanowires and graphene, enhancing the permittivity of the metal/graphene networks. Free-standing GO/Ag nanowire films achieved an EMI SE of up to 62 dB within the 8–40 GHz range [50]. The shielding mechanism involved multiple reflections and absorption of EMWs due to the oxygen-containing GO and conductive Ag nanowire layers. The random distribution of charge concentration and electron cloud density increased dipole polarization relaxation.

4.6.3 Graphene-polymer composites

Graphene materials have been extensively combined with various polymers to create composites with superior mechanical strength, high conductivity, and improved shielding performance [51]. In these composites, graphene materials act as fillers, enhancing conductivity and permeability. The filler fraction significantly impacts the composite's mechanical and EMI shielding characteristics. High filler content can make the composite brittle with poor mechanical strength; therefore, research has focused on improving shielding performance with low filler content.

Graphene and metals are widely considered the best composites for EMI shielding; however, they come with certain limitations. With advancements in electronic applications, there is an increasing demand for effective shielding materials that offer thermal expansion, design flexibility, and noncorrosive properties. Additionally, the weight-to-strength ratio of EMI shielding materials is crucial from an inertia and structural perspective. Lightweight polymer composites have emerged as the most promising materials for these applications. Various methods have been employed to create polymer-based composites, such as solution processing, in situ growth, hydrothermal, Hummer's, and solvothermal methods. In the X-band frequency range, chemical vapor deposition has achieved the highest total SE of up to 90 dB. In the Ku-band, the highest total SE reached up to 60 dB with a reflection loss of −61.4 dB using the hydrothermal method. For the K-band frequency range, the maximum total SE of 51.4 dB, 51.1 dB, and 51 dB was achieved using the

ultrasonication technique, Hummer's method, and solution processing method, respectively, while the solution processing method also achieved a reflection loss of −61 dB. In the Ka-band frequency range, chemical vapor deposition yielded the highest total SE of 77 dB. This method provided superior shielding in both the X-band and Ka-band. Additionally, a high reflection loss of −78 dB was observed in the V-band frequency range using the ultrasonication method [48,52].

Gao et al. [53] created 3D graphene aerogel/polydimethylsiloxane (PDMS) composites through a bidirectional freezing process. With only 0.42 wt% graphene content, the composite exhibited a maximum EMI SE of 65 dB in the X-band region. The multiple lamellar interfaces contributed to enhanced shielding performance. An rGO material with a honeycomb structure dispersed in epoxy resin demonstrated a maximum EMI SE of 38 dB in the X-band, with a 1340-fold increase in conductivity compared to a standard rGO/epoxy composite, highlighting the honeycomb morphology's importance in promoting electron transport and multilevel EMI shielding [54].

The thickness of shielding samples plays a crucial role in shielding performance. Liang et al. developed a polyvinylidene fluoride (PVDF) film with a multilayered structure incorporating graphene nanosheets and nickel (Ni) nanochains. The film, with a thickness of 0.5 mm, exhibited an SE of 43.3 dB, which increased to 51.4 dB with a thickness of 0.7 mm [55]. The graphene presence significantly improved thermal conductivity by 1200% compared to a pure PVDF film. The multilayered composite displayed higher DC electrical conductivity than other material combinations. The increase in EMI SE with thickness is clearly visible, and the additional interfaces between Ni nanochains and graphene in the Ni/graphene/PVDF film enhanced EMW attenuation. The denser conductive layer in the film created a larger impedance mismatch and higher conductivity losses, significantly improving absorption and reflection SE.

4.6.4 Other types of graphene composite materials

Graphene materials have been extensively utilized as templates for growing metal oxides with diverse morphologies. Fe_3O_4, known for its low toxicity, high magnetic properties, and enhanced dielectric and magnetic losses, has been widely integrated with graphene for effective EMI shielding applications. For instance, composites of hollow Fe_3O_4-filled 3D graphene foam and PDMS, as well as magnetic Fe_3O_4 nanoplatelets-coated rGO with conductive epoxy polymer, have demonstrated significant improvements in EMI SE [56]. Additionally, PVDF-based graphene/Fe_3O_4 composite films have shown high flexibility and enhanced SE retention after multiple bending-release cycles. The synthesis methods, such as combining thermally annealed graphene with ethylenediamine-functionalized Fe_3O_4, play a crucial role in determining the properties and performance of the resulting materials. Comparative studies highlight the importance of porosity in shielding performance, and the use of metal–organic frameworks (MOFs) as precursors has led to the development of advanced composites like MIL-88 B-derived Fe_3O_4–C and graphene nanoplates [57]. By increasing the number of layers in composite films, both conductivity and EMI SE are enhanced, with Fe_3O_4 acting as an efficient EMW absorber. The integration of

Fe_3O_4 with graphene and MWCNTs, along with PEG-based block copolymer, has further advanced the development of self-healing EMI shielding materials.

In addition to Fe_3O_4, graphene has been combined with another iron oxide, Fe_2O_3, to create effective EMI shielding composites. For instance, Wang and colleagues fabricated γ-Fe_2O_3/graphene composites through a solvothermal process, achieving enhanced MW absorption in the S band and C band due to good impedance matching [58]. In another study, graphene was combined with γ-Fe_2O_3/C nanoparticles to develop core-shell composites that achieved a reflection loss of 38.2 dB at a thickness of 2.5 mm. Notably, with a 20% filling content, the composite could cover 98% of the Ku-band with a thickness of 2.2 mm [59]. The layered structure of rGO favors multichannel reflection paths, while metal oxide nanoparticles boost MW loss capacity. Additionally, metal sulfides have been combined with graphene derivatives. For example, hydrothermally synthesized CuS/rGO composites using GO and copper dithiooxamide complex exhibited good EMI shielding performance. The composite with 9 wt% copper dithiooxamide showed an EM SE of 64 dB at 2.3 GHz. For frequencies between 2 and 8 GHz, the average absorption-dominant EMI SE of the CuS/rGO nanocomposite (12 wt% copper dithiooxamide) ranged from 45 to 54 dB. These studies underscore the potential of graphene materials as ideal candidates for EMI shielding applications.

The physical or chemical processes involved in the composite's formation determine its EMI shielding and other parameters [60]. For example, a composite made of thermally reduced graphene oxide-carbon nanotubes (TG-CN) and poly(methyl methacrylate) (PMMA) displays an EMI SE of 30.4 dB, whereas a chemically reduced GO-carbon nanotube/PMMA composite has 1.68 times less EMI SE.

Yang et al. created an epoxy copper nanowires/thermally annealed graphene aerogel composite, achieving an EMI SE of 47 dB with electrical conductivity (EC) of 1.208 S/cm at a 2 mm thickness [61]. Introducing copper significantly improved the EMI SE compared to pure epoxy resin. Liang et al. reported a 32.5 dB EMI SE for graphene/SiC-nanowires/poly(vinylidene fluoride) composites with a thickness of 1.2 mm and EC of 0.015 S/cm. Adding inorganic components to the composite influences its EMI SE, EC, magnetic properties, and reflection loss. For instance, cobalt-rich glass-coated microwires combined with a graphene/silicone rubber composite can block 98.4% of incident radiation with a filler loading of 0.059 wt.% [62].

Nickel foam, fabricated using a solution combustion technique, was enhanced with rGO to form a remarkable EMI shielding structure. This Ni-rGO foam achieved a maximum reflection loss of −53.11 dB, showcasing high porosity and dielectric loss. Similarly, Fe_3O_4/graphene-coated Ni foam/poly dimethylsiloxane composites demonstrated an EMI SE of 32.4 dB with EC of 2.5 S/cm. Polyurethane-based GN composites, such as polyurethane/graphene (PUG20) with 20 wt.% graphene, effectively block 98.7% of incident radiation [61,63].

Pyrolysis of GN-based polymer composites enhances EMI shielding and parameters like EC, dielectric properties, and permeability. For example, CNTs codecorated porous carbon/graphene/PDMS foam generate 48 dB of shielding ability with a specific SE of 347.8 dB/g·cm^3. Higher annealing temperatures repair defects and improve ohmic loss. Additionally, metal nanoparticle decoration with GN in a polyaniline

(PANI) matrix significantly improves EMI SE compared to GN/PANI in a polyimide matrix [64].

LDHs and their composites have shown great potential as photocatalysts for the treatment of organic pollutants in industrial wastewater [65]. Adding GO content in composite photocatalysts provides an efficient pathway for charge separation. The mass ratio of GO to LDH significantly impacts the morphological characteristics of these hybrid materials. GO/LDH hybrids exhibit hierarchical morphologies formed through in situ crystallization and ex situ hybridization. Functional groups on GO help in the adsorption of metal cations and direct the development of LDH crystallites during in situ crystallization. During ex situ hybridization, exfoliated GO and LDH materials interact closely, resulting in the arrangement of different GO and LDH sheets, forming successive layers of GO/LDH nanohybrids [66]. Two orientations of LDHs—vertical and parallel—were observed on the GO surface. The amount of LDH crystallites increases with a higher ratio of LDH nuclei to GO. At low LDH ion concentrations, LDH crystallites develop in both vertical and parallel orientations on the GO surface, while at high concentrations, they only develop vertically. Uniformly deposited LDH crystallites on GO exhibit a hexagonal shape and show a mixture of vertical and parallel orientations at varying LDH concentrations. Rosaiah and colleagues developed flower-like RGO/LDH nanocomposites for high-performance asymmetric supercapacitors using a one-pot scheme [67]. FESEM images clearly display the formation of flower-like layered architecture in the NC/RGO-LDH composites, while TEM images show RGO composited with NC-LDH without disturbing its basic architecture. SAED patterns indicate well-defined diffraction circles in the composites, consistent with XRD results. Jung and team showed that laser-assisted patterning of RGO/CoNi-LDH composites enhances microsupercapacitor performance [68].

4.6.5 MXene

MXenes, as a novel kind of 2D materials consisting of transition metal carbides/nitrides, were developed in 2011. Represented by the formula Mn+1BnTx (where M is a transition metal like Ti, V, or Mo, B is C or N, and Tx represents functional groups like –OH, –O, –F), MXENEs exhibit unique electronic, optical, mechanical, and colloidal properties. They have high conductivity (~15 kS/cm for Ti_3C2Tx) and absorb 3% of visible light per nanometer thickness, making them optically transparent. With a modulus of elasticity between 330 and 400 GPa, these materials are used in sensors, energy storage devices, and EMI shielding devices [69].

MXenes offer a promising alternative to carbon-based nanomaterials to compensate for their poor dispersion and limited compatibility with polymer matrices. With abundant surface functional groups, they enhance compatibility and interfacial interaction with polymers. Additionally, MXenes possess outstanding electrical conductivity, mechanical strength, and a planar structure that provides a large surface area, effectively absorbing and reflecting EMWs. Composites of MXene and graphene are prepared using various methods such as vacuum-assisted filtration (VAF), dip coating, spray coating, solvent casting, freeze drying, and spin coating.

The chosen process depends on the composition, purpose, and type of material used. In the VAF technique, a homogenized mixture is filtered and dried using sonication or stirring, with filters made from paper, nylon, polypropylene, or polycarbonate. Hybrid films can also be created by alternating filtration of the homogenized mixture. In the dip coating process, matrix materials are immersed in a suitable solvent for a specific time and then dried, and the cycle is repeated as needed. Spray coating follows a similar process, where spraying speed, time, solvents, pressure, and particle size are controlled to meet product quality requirements [70]. Fig. 4.4 presents fabrication methods of nanocomposite films for EMI shielding purposes [71].

(A) Schematic of the fabrication of PVA/MXene alternating multilayered film through multilayered casting. (B) Schematic of EM MW dissipation in the PVA/MXene multilayered films. Schematic of thermal conductive pathway contributing to the high thermal conductivity in the PVA/MXene multilayered. (D) Schematic diagram of EMI shielding mechanism for Ti3C2Tx/rGO porous EMI shielding composite films [71].

Solvent casting involves evaporating the solvent from the homogenized mixture in an air or vacuum oven, after which the film is separated from the casting plate. Freeze drying entails freezing a homogenized water mixture under liquid nitrogen and drying it at the same temperature. This results in various structures like honeycomb, porous, and foam composites, which depend on the elements present in the mixture. Finally, spin coating is a common method used to prepare thin electronic devices. It involves high rpm, different substrates, and evaporation techniques to achieve the desired outcome [72].

MXenes contain tough covalent and metallic bonds within their MAX phase, making them difficult to break. During MXene synthesis, etchants like hydrofluoric acid, ammonium hydrogen bifluoride, or a mix of lithium fluoride and hydrochloric acid are used to break these metallic bonds, resulting in multilayered MXene. After etching, multilayered MXene can be dispersed in dimethyl sulfoxide to form colloidal solutions, which are then processed into composites, coatings, and films. Dimethyl sulfoxide swells the layered MXene structure, increasing inner layer spacing and weakening interlayer bonds. Sonication disperses and delaminates the multilayered MXene into nanosheets [73]. Additionally, lithium fluoride can be used to create lithium-ion-intercalated MXene, which swells in water during a direct ion exchange process. Manual shaking of multilayered MXene in water produces large MXene flakes with fewer defects than sonication. The mechanical properties of MXenes, like those of LDHs, depend on surface functional groups, with oxygen-terminated MXenes exhibiting significant tensile strength and toughness [74].

It is worth noting that, similar to MXenes, the electrostatically self-assembled 2D/2D heterostructure of GO and MXenes has demonstrated excellent physicochemical, thermomechanical, EM, and electronic properties, making them highly suitable for potential energy storage applications. Also, recently, Ti3C2Tx MXene is ingeniously assembled into the 3D macroscopic hydrogel under mild conditions by a GO-assisted self-convergence process [75].

MXenes, as 2D materials, hold great promise for 3D printing applications because of their hydrophilic nature and chemical reactivity, thanks to surface functional

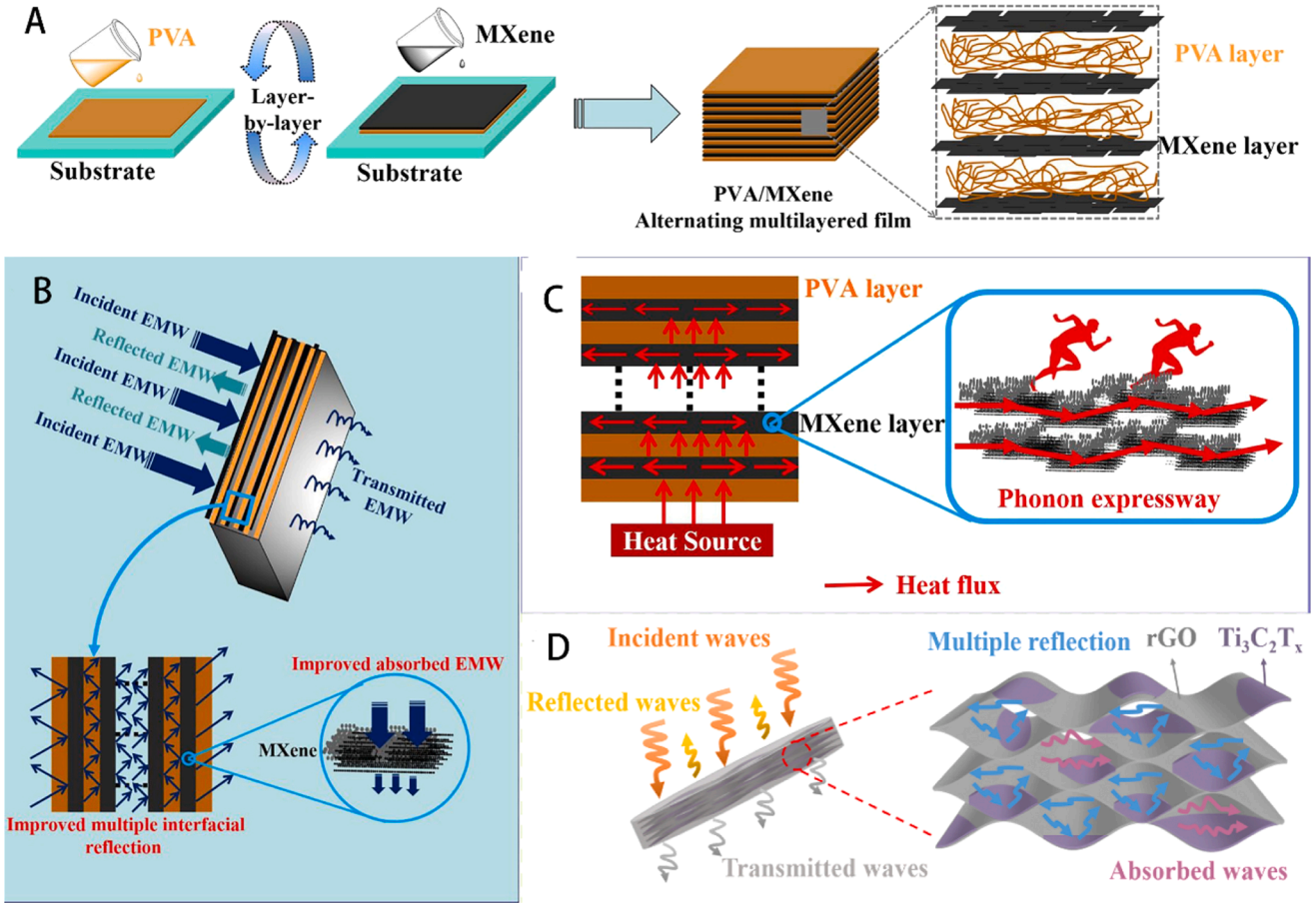

Figure 4.4 Fabrication of nanocomposite films for EMI shielding purposes (A) schematic of the fabrication of PVA/MXene alternating multilayered film through multilayered casting. (B) Schematic of electromagnetic microwave dissipation in the PVA/MXene multilayered films. (C) Schematic of thermal conductive pathway contributing to the high thermal conductivity in the PVA/MXene multilayered. (D) Schematic diagram of EMI shielding mechanism for Ti3C2Tx/rGO porous EMI shielding composite films. Fabrication of nanocomposite films for EMI shielding purposes.

From Z. Xiangyu, Z. Haiwei, L. Zhihao, J. Rijia, Z. Xing, Functional composite electromagnetic shielding materials for aerospace, electronics and wearable fields, Materials Today Communications 33 (2022) 104498.

groups such as —OH, —O, or —F. This unique combination makes them ideal for colloidal processing, which involves dispersing particles in a liquid medium without compromising their electrical properties. Zhou and coworkers were able to modify the rheology properties of MXene by using cellulose nanofibers (CNF) as an additive [76].

Chang and colleagues explored the creation of a hierarchical porous CNT-bridged MXene (MXene/CNT) skeleton using a straightforward freeze-drying method. They utilized melamine foam (MF) with a low-density, 3D porous structure as the substrate. Subsequently, small amounts of CNT were added to connect the weak MXene layers. The freeze-drying process effectively bridged the porous CNT with the MXene skeleton (MXene/CNT), resulting in effective EMI shielding of 34.7 dB for a wide range of multifunctional applications [77].

Nanocomposites also hold great promise for high-sensitivity and precision instrumentation. Jin and colleagues developed a polyvinyl alcohol (PVA)/MXene film with an alternating multilayered structure using multilayered casting [78]. The layered MXenes provide excellent electrical and thermal conductivity, absorbing EMWs through multiple reflections and dissipating them as heat. This outstanding thermal conductivity prevents damage from heat accumulation and overheating. Additionally, the composite exhibits excellent fire resistance and drip resistance. During combustion, MXene forms a protective TiO_2 layer on the surface, effectively preventing flame spread and diffusion, while maintaining the film's structural integrity [79].

To address the challenge of forming a highly conductive network with MXene nanosheets in a homogeneous film, Zhou and team designed an asymmetric sandwich structural film. This film includes a CNF skin-layer, a self-supporting MXene layer, and silver nanowire (AgNW) core-layers. The resulting composite material is ultra-flexible, has high tensile strength, and exhibits unique properties due to its sandwich structure [79].

4.6.6 TMDs

TMDs are a family of thin semiconducting materials with the formula MX_2, where M represents transition metals like molybdenum (Mo), tungsten (W), vanadium (V), and others, while X represents chalcogen atoms such as sulfur (S), selenium (Se), and tellurium (Te). The transition metal layer is sandwiched between layers of chalcogen atoms, typically with a metal layer thickness of 6–7 Å. Due to their excellent electrical and chemical properties, high charge carrier mobility, low power consumption, flexibility, stretchability, lightweight nature, mechanical robustness, and environmental stability, these materials are well-suited for flexible gas sensing applications [80]. The charge transfer between the dichalcogenide material and the target gas is critical to the sensing mechanism of TMDs. Changes in the electrical conductivity of TMDs are primarily influenced by whether the target gas is oxidizing or reducing. These materials are typically synthesized using high-temperature chemical vapor deposition, which is not ideal for direct growth on a substrate. As a result, traditional methods are employed to transfer the 2D material onto a flexible substrate [81]. Most promising material MoS_2 shows excellent gas adsorption, high flexibility, and transparency

aspects, making it a leading candidate for emerging flexible gas sensing technology. Several methodologies have been adopted for the synthesis of mono- and few-layer MoS_2 films, including micromechanical exfoliation, wet chemical processes, chemical or physical vapor deposition, and pulsed laser deposition [82]. The morphology of deposited MoS_2 can be easily tailored by changing the synthesis technique. For instance, nanobelts, nanoribbons, nanorods, and nanoflowers have been fabricated using various fabrication methods [83].

4.7 Measurements of EM properties of 2D materials in composites

The interaction between EM waves and absorbing materials results in various types of losses. These interactions can be attributed to electronic effects caused by the electric field component of the wave, leading to dielectric losses, or to magnetic interactions due to the time-varying magnetic field. These interactions can also be a combination of both electronic and magnetic effects. The behavior of EM waves and their interactions can be described by Maxwell's equations, considering appropriate boundary conditions [81,84].

Dielectric losses are generated due to interfacial polarizations in materials, the formation of conductive networks, defects leading to defect-induced polarizations, and dipolar relaxation processes. Interfacial polarization arises from homogeneous or heterogeneous interfaces in the host material due to differences in dielectric and conductive properties. Structures like porous, core-shell, and hollow forms also contribute to interfacial polarization. The presence of air within the material creates different dielectric properties, leading to interfacial polarization [85].

Nanostructured oxide semiconductors are used in energy conversion, catalysis, sensing, and environmental applications exploiting the techniques that include oxygen vacancy utilization and heteroatom doping [86]. Oxygen vacancy defects are common in materials containing oxygen with low formation energy. When an EM wave interacts with these sites, charge carriers generated by the external EM field get trapped, causing polarization effects due to charge accumulation or imbalance [87].

Carbon-based materials like carbon fibers, carbon nanotubes, conducting polymers, and graphene exhibit high conductivity. The formation of conductive networks leads to Joule heating when electric current flows through these networks. Conductive losses appear as Joule heat effects due to internal resistance within the material. Two models explain conductive loss: the electron migration model, where electrons move freely within a conductive network of 1D (carbon nanotubes) or 2D (graphene sheets) materials, and the electron hopping model, where electrons transfer from one interface or defect to another [88,89].

Conduction losses can also be explained using free electron theory, where the loss factor (ε'') is proportional to the material's conductivity (σ) and the frequency of the external EM wave (f). High conductivity can cause impedance mismatching between the material and free space, increasing EM wave reflection instead of attenuation.

Therefore, while higher conductivity can increase dielectric loss, it must be optimized to prevent excessive conduction currents and maintain effective MA [90].

These loss mechanisms are crucial for designing materials with optimal MA properties, ensuring broad bandwidth, high reflection loss (RL), and minimal thickness or weight.

2D materials like graphene, MXENE, MoS_2, and WeS_2 are increasingly being used in flexible electronic wearable devices due to their excellent physical, mechanical, and chemical properties. These materials are also considered ideal for MA applications. During synthesis, surface modifications and various structural assemblies are developed, which lead to defects, resulting in induced polarization effects, excellent dielectric losses, and magnetic conductive losses [91].

Chemically reduced graphene (CR-G) combined with poly-(ethylene oxide) (PEO) has shown effective MA, with a maximum reflection loss of −38.8 dB at 17 GHz for a 1.8 mm thickness and an effective bandwidth of around 4.5 GHz [92]. rGO in a nitrile butadiene rubber (NBR) matrix, prepared by thermal exfoliation, demonstrated a maximum reflection loss of −57 dB at 9.6 GHz for a 10 wt% rGO content, with an effective bandwidth of 4.5 GHz at 3 mm thickness. The excellent absorption properties were attributed to the layered and porous structure, which resulted in multiple reflections and increased loss [93].

Ultrathin graphene composites have shown varied MA properties with temperature changes. At 473 K, a maximum reflection loss of −42 dB was achieved, covering the entire X-band, due to the presence of functional groups and dipolar polarization, conductive network formation, and decreased friction between layers. Nitrogen-doped graphene, prepared by a hydrothermal process, exhibited good magnetic properties and improved MA due to good impedance matching and polarization relaxation, achieving a maximum reflection loss of −11.30 dB at 12.7 GHz with an effective bandwidth of 2.1 GHz [94].

A novel graphene-coated Fe-nanocomposite, prepared by the Modified Hummer method followed by hydrothermal and reduction reactions, showed excellent absorption properties with a maximum reflection loss of −45 dB at 7.1 GHz for a 2 mm thickness and an effective bandwidth of 4.4 GHz [95]. Additionally, RGO/MnFe2O4/PVDF (polyvinylidene fluoride) composites and rGO loaded with irregular magnetic quantum dots (MQDs) have demonstrated excellent MA properties due to the presence of both dielectric and magnetic losses and good impedance matching [96].

Overall, graphene-based composites exhibit promising MA properties, making them suitable for various applications in flexible electronics and other advanced technologies.

Recent studies have explored MXENEs as promising materials for sensors, energy storage devices, EMI shielding devices and MW absorbers [84].

Significant research is currently focused on developing innovative, high-capacitance MXene-based materials for supercapacitor electrodes. MXenes such as Ti_3C_2, Mo_2C, Ti_2C, and $Mo_{1.33}C$ have demonstrated remarkable electrochemical properties as supercapacitor electrode materials [97].

Qing Yuchang et al. [98] investigated the MA properties of titanium carbide (Ti_3C_2) MXene nanosheets, synthesized by treating Ti_3AlC_2 with HF powder under ultrasonication. Their comparative study revealed that Ti_3C_2 exhibited superior absorption properties compared to Ti_3AlC_2, achieving a maximum reflection loss of −17 dB at a resonance frequency of 14.60 GHz, with an effective bandwidth of 5.5 GHz covering the entire Ku-band. The exceptional performance was attributed to the unique structure, layer capacitance, and numerous defects.

Wanlin Feng et al. [99] developed a Ni-doped Ti_3C_2 MXene composite by first treating Ti_3AlC_2 with HF and then doping it with nickel through a chemical method. Morphological analysis revealed an accordion-like structure. The composite's synergistic dielectric and magnetic loss properties enabled excellent impedance matching, resulting in enhanced MA. The composite achieved a reflection loss of −17.5 dB with an effective bandwidth of 6.3 GHz at a matching thickness of 1.5 mm [100]. Ji Liu et al. [101] created a 3D lightweight aerogel composed of MXene sheets interconnected with polyimide macromolecules. The composite demonstrated exceptional mechanical and electrical properties. It exhibited a reflection loss of −45.5 dB with an effective bandwidth of 5.1 GHz. The composite's excellent mechanical flexibility and conductivity make it a strong candidate for MW absorbers.

Two-dimensional transition metal dichalcogenides (2D-TMDs) have a wide range of potential applications, including sensors, field-effect transistors (FETs), energy storage devices, and photodetectors. Recent studies have shown that 2D-TMDs are also effective in MW-absorbing materials due to their chemical activity, excellent electrical conductivity, and suitable band gap for MA [102]. While pristine TMDs exhibit decent absorption losses, their performance can be further enhanced by forming composites with other materials. Studies on the MA properties of MoS_2 and WS_2 find that MoS_2 nanosheets synthesized via the hydrothermal method display varying morphologies based on the hydrothermal temperature [103].

A 3D hierarchical heterojunction of MoS_2/FeS_2 prepared through the hydrothermal route demonstrated the best MA properties with a 2:5 M ratio of MoS_2:FeS_2. This composite, with a reflection loss of −60.2 dB and an effective bandwidth of 6.48 GHz, benefited from polarization effects, multiple reflections, scattering, and high conductivity [104]. The $NiS_2@MoS_2$ composite, featuring a core-shell structure confirmed by SEM and TEM images, achieved a maximum reflection loss of −41.05 dB and an effective bandwidth of 4.4 GHz. The loss mechanisms included dipolar and interfacial polarization, multiple reflections, quarter-wavelength matching, and good impedance matching [105].

MoS_2/Graphene heterostructure enhanced impedance matching, leading to multiple reflections between the layers and defects in the layers. The composite exhibited improved MA properties due to the presence of a heterostructure. MoS_2/graphene heterostructure facilitated Mg-diffusion kinetics for high-performance rechargeable magnesium batteries [106].

Overall, the combination of TMDs with other materials significantly enhances their EM capabilities, making them promising candidates for various applications.

Carbon nanomaterial combined with WS_2, MoS_2, or $BaTiO_3$ nanoparticles improves the composite's dielectric properties. Mixing nanocarbon fillers with magnetic

particles, such as ferrite or metal (alloy) particles, enhances carbon-filled composites' absorptive properties. Ferrite particles offer advantages like high ferromagnetic resonance frequency, high electric resistivity, low density, and good chemical stability. Adding magnetic particles like Fe_2O_3, Fe_3O_4, $MnFe_2O_4$, ZnO hollow spheres or nanoparticles, Co_3O_4, and MnZn-ferrite can enhance EMR SE and reduce NC costs. For example, coating CNTs with Fe_3O_4 achieved a specific RLmin of 28.7 dB and an effective bandwidth of 8.3 GHz. Microstructured fillers combining graphene and carbon nanotubes with magnetic Fe_3O_4 particles have shown excellent absorbing properties, demonstrating their potential as EMR absorbing materials [107]. A CNT film- Fe_3O_4-rGO-polydimethylsiloxane (PDMS) composite with four layers achieved a maximum RL of 50.5 dB and an absorption bandwidth of 5.7 GHz at a thickness of 1.42 mm [108].

Boron nitride nanosheet (BNNS)-polymer composites are a significant class of materials with diverse applications, including automotive, aerospace, healthcare, medicine, energy storage, and electronic engineering [109]. While extensive efforts have been made to incorporate graphene into polymer materials, BNNS-polymer composites have received less attention. Boron nitride (BN) nanomaterials offer exceptional properties, including superior fracture strength (165 GPa), high Young's modulus (0.8 TPa), excellent thermal stability (up to 800°C in the air), an outstanding thermal expansion coefficient (-2.72×10^{-6}/K), and remarkable thermal conductivity (300–2000/Wm/K). Unlike other 2D materials like graphene and MXene, BNNS is electrically insulating due to its wide bandgap (~5.6 eV), dielectric constant (4–8), low leakage current, and high voltage breakdown strength (12 MV/cm). Large-scale production of boron nitride nanosheets is being researched for flexible thermal interface materials and advanced dielectrics necessary to catch up to the rapid development and miniaturization of electronic devices, integration, multi-functionalization, the device stability and reliability [110].

4.8 Conclusions and outlook

Significant progress in nanomaterials and nanotechnology has opened new avenues for research across various disciplines. The unique scale effects of nanomaterials give rise to unexpected macroscale phenomena and properties, enabling a wide range of applications. However, the process of multifunctionalization can introduce both physical and commercial constraints. As a result, research must expand in diverse directions, including sensors, actuators, energy harvesters, and solar cells, with research efforts aimed at boosting sensitivity and enabling untethered communication.

Currently, there is significant development in radio frequency (RF) and MW electronics, including mobile communications, high-speed electronic switching components and circuits, radars, and navigation systems. To ensure the proper operation of these devices, nearby electronic equipment operating in the RF and MW frequency bands must be adequately shielded, often by coating the device case with shielding material. Many high-frequency electronic devices operate in the X-band

(8–12 GHz) of the EM spectrum. As communication standards evolve, there is a need for new, effective materials capable of high-speed data transmission, operating within the 20–100 GHz frequency range.

Furthermore, the development of soft and flexible electronic devices, such as foldable phones, electronic paper displays, and wearable devices, requires thin and flexible EMR shielding films. Next-generation EMR shielding materials will likely involve seamlessly networked hetero-nanostructures, the composition of which is the subject of extensive modern research. Structured organic-inorganic composites are widely studied due to their combination of inorganic materials' advantages (electric and magnetic properties, mechanical strength, and thermal stability) and organic polymers' benefits (dielectric properties, processability, flexibility, and ductility). These composites enhance EM absorption efficiency.

Carbon nanomaterials and polymer nanocomposites have numerous advantages for wideband EMI shielding applications, including high SE, light weight, flexibility, high conductivity, and low contact resistance. However, they have limitations as MW absorbers, such as requiring a large volume of filler for strong MW absorption, which can deteriorate filler dispersion and affect mechanical properties. A conductive network with increased filler content may limit MA and restrict the effective bandwidth (EB). Obtaining high EMR SE for polymer/conductive filler composites is challenging, especially when using a single type of conductive filler. Adding another inorganic filler can enhance EMR absorption.

Numerous EMI composite shielding materials have been extensively developed. However, the mechanisms governing the reflection and absorption of EMWs within shielding materials require further investigation. Advancing the understanding of these mechanisms is essential for enhancing the development and effectiveness of shielding materials.

Acknowledgments

This research was supported by the European Union's Horizon Europe Coordination and Support Actions programme under grant agreement No 101079151 - GrInShield. D. K. thanks the Ministry of Science, Technological Development, and Innovations of the Republic of Serbia (grant number 451-03-136/2025-03/200017).

Part of this work was supported over the years in part by NIH grants 1 R01 CA259635-01A1 and 3 R01 CA243033- 03S1A1, National Science Foundation (NSF) award #2153425, the Army Research Office through the ARO- (Contract Nos. W911NF-18-1-0076, W911NF2010103, and W911NF1910369, ARO-MURI program and AROCore grants no. MURI W911NF-11-1-0024, ARO W911NF-09-1-0319), the French American Cultural Exchange (FACE) Partner University Fund program, and the Air Force Office of Scientific Research (AFOSR) under awards FA9550-23-1-0061 and FA9550-23-1-0436 Any opinions, findings, and conclusions or recommendations expressed in this material are those of the author(s) and do not necessarily reflect the views of the United States Air Force.

References

[1] M.-S. Cao, X.-X. Wang, M. Zhang, J.-C. Shu, W.-Q. Cao, H.-J. Yang, X.-Y. Fang, J. Yuan, E. Response, E. Conversion, For functions and devices in low-dimensional materials, Adv. Funct. Mater. 29 (2019) 1807398.

[2] H. Chaudhuri, Y.-S. Yun, A critical review on the properties and energy storage applications of graphene oxide/layered double hydroxides and graphene oxide/MXenes, J. Power Sources 564 (2023) 232870.

[3] E. Garnett, L. Mai, P. Yang, Introduction: 1D nanomaterials/nanowires, Chem. Rev. 119 (15) (2019) 8955–8957.

[4] R.S. Wagner, W.C. Ellis, Vapor-liquid-solid mechanism of single crystal growth (new method growth catalysis from impurity whisker epitaxial + large crystals Si E, Appl. Phys. Lett. 4 (1964) 89–90.

[5] P.D. Yang, C.M. Lieber, Nanorod-superconductor composites: a pathway to materials with high critical current densities, Science 273 (1996) 1836–1840.

[6] S.P. Jovanović, Z.M. Marković, D.N. Kleut, M.D. Dramićanin, Structural analysis of single wall carbon nanotubes exposed to oxidation and reduction conditions in the course of gamma irradiation, J. Phys. Chem. C 118 (29) (2014) 16147–16155.

[7] A. Machín, K. Fontánez, J.C. Arango, D. Ortiz, J. De León, S. Pinilla, V. Nicolosi, F. I. Petrescu, C. Morant, F. Márquez, One-dimensional (1D) nanostructured materials for energy applications, Materials 14 (10) (May 17, 2021) 2609.

[8] N.P. Dasgupta, J.W. Sun, C. Liu, S. Brittman, S.C. Andrews, J. Lim, H.W. Gao, R. X. Yan, P.D. Yang, 25th anniversary article: semiconductor nanowires synthesis, characterization, and applications, Adv. Mater. 26 (2014) 2137–2184.

[9] L. Yu, et al., Graphene and beyond: recent advances in two-dimensional materials synthesis, properties, and devices, ACS Nanosci. 2 (6) (2022) 450–485.

[10] D. Kleut, M. Milenkovic, A. Pantic, F. von Kleist-Retzow, M. Sebbache, K. Haddadi, S. Jovanovic, Microwave electromagnetic shielding with free-standing composites based on graphene oxide and silver nanowires, J. Micro Bio Robot. 20 (2024) 13. Chaudhuri and Yun, no date.

[11] M. Huskić, D. Kepić, D. Kleut, M. Mozetič, A. Vesel, A. Anžlovar, D.B. Bogdanović, S. Jovanović, The influence of reaction conditions on the properties of graphene oxide, Nanomaterials 14 (3) (2024) 281.

[12] J.R. Prekodravac, M.D. Budimir, D.N. Kleut, B.R. Vasiljević, V.B. Rajić, G. Ciasca, B. M. Todorović Marković, Surface functionality as a key parameter for the conductivity of microwave synthesized CQDs thin films", Diam. Relat. Mater. 129 (2022) 109366.

[13] D.P. Kepić, D.N. Kleut, Z.M. Marković, D.V. Bajuk-Bogdanović, V.B. Pavlović, A. J. Krmpot, M.M. Lekić, D.J. Jovanović, B.M. Todorović-Marković, One-step preparation of gold nanoparticles - exfoliated graphene composite by gamma irradiation at low doses for photothermal therapy applications, Mater. Char. 173 (2021) 110944.

[14] M. Budimir, D. Kleut, B.T. Markovic, R. Boukherroub, Reduced graphene oxide-chitosan flexible nanocomposites for efficient bacteria capture and photothermal ablation, Resolut. Discov. 5 (2020) 5–12. Cao et al., 2019.

[15] D. Kepić, Z. Marković, S. Jovanović, I. Holclajtner Antunović, D. Kleut, B. Todorović Marković, Novel method for graphene functionalization, Phys. Scrip. Top. Iss. T162 (2014) 014024.

[16] Z. Markovic, D. Kleut, B. Babic, I. Holclajtner-Antunovic, Carbon-doped cryogel thin films derived from resorcinol formaldehyde, Advan. Carb. Mater. Technol. (2013) 475.

[17] D.N. Kleut, Z.M. Markovic, B.M. Babić, I.D.H. Antunović, Raman spectroscopy study of carbon-doped resorcinol-formaldehyde thin films, Phys. Scrip. T157 (2013) 014039.
[18] Y. Shi, M. Wu, S. Ge, et al., Advanced functional electromagnetic shielding materials: a review based on micro-nano structure interface control of biomass cell walls, Nano-Micro Lett. 17 (2025) 3.
[19] R. Khan, Z.M. Khan, H.B. Aqeel, et al., 2D nanosheets and composites for EMI shielding analysis, Sci. Rep. 10 (2020) 21550.
[20] Nguyen, Quy-Dat, et al., Recent advances in multifunctional electromagnetic interference shielding materials, Heliyon 10 (10) (2024) e31118.
[21] E. Stern, F. James, Klemic, A. David, Routenberg, N. Pauline, Wyrembak, B. Daniel, Turner-Evans, D. Andrew, Hamilton, A. David, LaVan, M. Tarek, Fahmy, M.A. Reed, Label-free immunodetection with CMOS-compatible semiconducting nanowires, Nature 445 (7127) (2007) 519–522.
[22] G. Hou, L. Zhang, V. Ng, Z. Wu, M. Schulz, Review of recent advances in carbon nanotube biosensors based on field-effect transistors, Nano Life 6 (2016) 1642006, 03n04.
[23] E.L. Muetterties, T.N. Rhodin, E. Band, C.F. Brucker, W.R. Pretzer, Clusters and surfaces, Chem. Rev. 79 (2) (1979) 91–137.
[24] Intel.
[25] F. Soler, V. Manuel, Fabrication and Characterization of Macroscopic Graphene Layers on Metallic Substrates, 2014.
[26] H. Tigelaar, The incredible shrinking IC: Part 3 BEOL Aluminum alloy single and Multilevel metal, How Transistor Area Shrank by 1 Million Fold (2020) 227–252.
[27] C. Rutherglen, P. Burke, Nanoelectromagnetics: circuit and electromagnetic properties of carbon nanotubes, Small 5 (8) (2009) 884–906.
[28] D.Y. Joh, J. Kinder, L.H. Herman, M.A. Sang-Yong Ju, Segal, N. Jeffreys, Johnson, J. Park, Single-walled carbon nanotubes as excitonic optical wires, Nat. Nanotechnol. 6 (1) (2011) 51–56.
[29] S. Li, Z. Yu, C. Rutherglen, P.J. Burke, Electrical properties of 0.4 cm long single-walled carbon nanotubes, Nano Lett. 4 (10) (2004) 2003–2007.
[30] Nair, R. Rahul, B. Peter, N. Alexander, Grigorenko, S. Konstantin, Novoselov, T. J. Booth, T. Stauber, N. Mr Peres, A.K. Geim, Fine structure constant defines visual transparency of graphene, Science 320 (5881) (2008), 1308–1308.
[31] F.H.L. Koppens, E. Darrick, Chang, F. Javier García de Abajo, Graphene plasmonics: a platform for strong light–matter interactions, Nano Lett. 11 (8) (2011) 3370–3377.
[32] F. Zhe, A.S. Rodin, O. Gregory, Andreev, W. Bao, A.S. McLeod, M. Wagner, L. M. Zhang, et al., Gate-tuning of graphene plasmons revealed by infrared nano-imaging, Nature 487 (7405) (2012) 82–85.
[33] L. Ju, G. Baisong, H. Jason, G. Caglar, M. Michael, H. Zhao, A. Hans, Bechtel, et al., Graphene plasmonics for tunable terahertz metamaterials, Nat. Nanotechnol. 6 (10) (2011) 630–634.
[34] F. Rana, Graphene terahertz plasmon oscillators, IEEE Trans. Nanotechnol. 7 (1) (2008) 91–99.
[35] P.H.Q. Pham, W. Zhang, N.V. Quach, J. Li, W. Zhou, D. Scarmardo, E.R. Brown, P. J. Burke, Broadband impedance match to two-dimensional materials in the terahertz domain, Nat. Commun. 8 (1) (2017) 2233.
[36] P.H.Q. Pham, W. Zhou, V. Nhi, Quach, J. Li, Jian-Guo Zheng, P.J. Burke, Controlling nucleation density while simultaneously promoting edge growth using oxygen-assisted

fast synthesis of isolated large-domain graphene, Chem. Mater. 28 (18) (2016) 6511–6519.
[37] R. Kumar, S. Sahoo, E. Joanni, Composites based on layered materials for absorption of microwaves and electromagnetic shielding, Carbon 211 (2023) 118072.
[38] K. Chen, Q. Wang, Z. Niu, J. Chen, Graphene-based mateials for flexible energy storage devices, J. Energy Chem. 27 (1) (2018) 12–24.
[39] M. Yasir Khalid, R. Umer, Towards a new era of 2D materials-based multifunctional composite films: from innovation to evolution, Advan. Indus. Eng. Polym. Res. 8 (1) (2025) 76–112.
[40] S. Jovanović, M. Huskić, D. Kepić, et al., A review on graphene and graphene composites for application in electromagnetic shielding, Graph. 2D Mater 8 (2023) 59–80.
[41] D. Dhamodharan, V. Dhinakaran, H.-S. Byun, MXenes: an emerging 2D material, Carbon 192 (2022) 366–383.
[42] K. Kang, S. Chen, E.-H. Yang, 12-Synthesis of transition metal dichalcogenides, in: E.-H. Yang, D. Datta, J. Ding, G. Hader (Eds.), Micro and Nano Technologies, Synthesis, Modeling, and Characterization of 2D Materials, and Their Heterostructures, Elsevier, 2020, pp. 247–264.
[43] X. You, Q. Zhang, J. Yang, S. Dong, Review on 3D-printed graphene-reinforced composites for structural applications, Compos. Appl. Sci. Manuf. 167 (2023) 107420.
[44] W. Yu, L. Sisi, H. Yang, J. Luo, Progress in the functional modification of graphene/graphene oxide: a review, RSC Adv. 10 (26) (2020) 15328–15345.
[45] Chuan-Bing, et al., Electromagnetic interference shielding of graphene aerogel with layered microstructure fabricated via mechanical compression, ACS Appl. Mater. Interf. 12 (27) (2020) 30686–30694.
[46] L. Anderson, P. Govindaraj, A. Ang, A. Mirabedini, N. Hameed, Modelling, fabrication and characterization of graphene/polymer nanocomposites for electromagnetic interference shielding applications", Carbon Trends 4 (2021) 00047.
[47] M. Aman, P. Konduparty, S. Sharma, R.P. Srivastava, S. Bhattacharyya, V. Sharma, K. Balani, S. Krishn Jha, S. Omar, Layered double hydroxide based composites for energy storage applications: insights into supercapacitors and batteries, J. Energy Storage 116 (2025) 116093.
[48] S. Ayub, B.H. Guan, F. Ahmad, M.F. Javed, A. Mosavi, I. Felde, "Preparation methods for graphene metal and polymer based composites for EMI shielding materials: state of the art review of the conventional and machine learning methods", Metals 11 (2021) 1164.
[49] M. Milenković, W. Saeed, M. Yasir, D. Sredojević, M. Budimir, A. Stefanović, D. Bajuk-Bogdanović, S. Jovanović, "Study of graphene oxide and silver nanowires interactions and its association with electromagnetic shielding effectiveness", Int. J. Mol. Sci. 25 (2024) 13401.
[50] J. Hui, et al., Free-standing, anti-corrosion, super flexible graphene oxide/silver nanowire thin films for ultra-wideband electromagnetic interference shielding, J. Mater. Chem. A 9 (2021) 1180–1191.
[51] A. Tarhini, A.R. Tehrani-Bagha, Advances in preparation methods and conductivity properties of graphene-based polymer composites, Appl. Compos. Mater. 30 (2023) 1737–1762.
[52] R.J. Chandra, B. Shivamurthy, S.D. Kulkarni, M.S. Kumar, Hybrid polymer composites for EMI shielding application—a review, Mater. Res. Express 6 (2019) 082008.

[53] W. Gao, N. Zhao, T. Yu, J. Xi, A. Mao, M. Yuan, H. Bai, C. Gao, "High-efficiency electromagnetic interference shielding realized in nacre-mimetic graphene/polymer composite with extremely low graphene loading", Carbon 157 (2020) 570–577.
[54] P. Song, C. Liang, L. Wang, H. Qiu, H. Gu, J. Kong, J. Gu, Obviously improved electromagnetic interference shielding performances for epoxy composites via constructing honeycomb structural reduced graphene oxide, Compos. Sci. Technol. 181 (2019) 107698.
[55] L. Liang, P. Xu, Y. Wang, Y. Shang, J. Ma, F. Su, Y. Feng, C. He, Y. Wang, C. Liu, Flexible polyvinylidene fluoride film with alternating oriented graphene/Ni nanochains for electromagnetic interference shielding and thermal management, Chem. Eng. J. 395 (2020) 125209.
[56] H. Fang, H. Guo, Y. Hu, Y. Ren, P.-C. Hsu, S.-L. Bai, In-situ grown hollow Fe_3O_4 onto graphene foam nanocomposites with high EMI shielding effectiveness and thermal conductivity, Compos. Sci. Technol. 188 (2020) 107975.
[57] K. Arya, A. Kumar, R. Kataria, Recent advances in MOF-based composites for the detection and adsorptive removal of Pb(II) ions in aqueous phase", Mater. Today Sustain. 29 (2025) 101057.
[58] X. Kou, Y. Zhao, L. Xu, Z. Kang, Y. Wang, Z. Zou, P. Huang, Q. Wang, G. Su, Y. Yang, Y.M. Sun, Controlled fabrication of core–shell γ-Fe_2O_3@C–Reduced graphene oxide composites with tunable interfacial structure for highly efficient microwave absorption, J. Colloid Interface Sci. 615 (2022) 685–696.
[59] K. Raagulan, B.M. Kim, K.Y. Chai, Recent advancement of electromagnetic interference (EMI) shielding of two dimensional (2D) MXene and graphene aerogel composites, Nanomaterials 10 (2020) 702.
[60] H. Chaudhuri, Y.-S. Yun, A critical review on the properties and energy storage applications of graphene oxide/layered double hydroxides and graphene oxide/Mxenes", Journal of Power Sources, Volume 564 (2023) 232870.
[61] X. Yang, S. Fan, Y. Li, Y. Guo, Y. Li, K. Ruan, S. Zhang, J. Zhang, J. Kong, J. Gu, "Synchronously improved electromagnetic interference shielding and thermal conductivity for epoxy nanocomposites by constructing 3D copper nanowires/thermally annealed graphene aerogel framework", Compos. Appl. Sci. Manuf. 128 (2020) 105670.
[62] C. Liang, M. Hamidinejad, L. Ma, Z. Wang, C.B. Park, "Lightweight and flexible graphene/SiC-nanowires/poly (vinylidene fluoride) composites for electromagnetic interference shielding and thermal management", Carbon 156 (2020) 58–66.
[63] C. Yu, S. Zhu, C. Xing, X. Pan, X. Zuo, J. Liu, M. Chen, L. Liu, G. Tao, Q. Li, Fe nanoparticles and CNTs co-decorated porous carbon/graphene foam composite for excellent electromagnetic interference shielding performance, J. Alloys Compd. 820 (2020) 153108.
[64] Y. Li, J. Liu, S. Wang, L. Zhang, B. Shen, Self-templating graphene network composites by flame carbonization for excellent electromagnetic interference shielding, Composites, Part B 182 (2020) 107615.
[65] M. Asif, M. Saeed, M. Zafar, U.-e-S. Amjad, A. Razzaq, W.Y. Kim, Development of Co-Al LDH/GO composite photocatalyst for enhanced degradation of textile pollutant under visible light irradiation, Results Phys. 42 (2022) 105997.
[66] D. Tonelli, E. Musella, E. Scavetta, M. Gazzano, V. Morandi, M. Christian, I. Gualandi, Design of nanohybrids based on layered double hydroxides and electrochemically reduced graphene oxide for energy applications, Catal. Today 427 (2024) 114401.
[67] P. Rosaiah, N. Guru Prakash, P. Divya, S. Sambasivam, M. Shkir, H. Algarni, T.J. Ko, One-pot synthesis of flower-like Ni-Co/reduced graphene oxide layered double

hydroxide nanocomposites as advanced electrodes for high-performance asymmetric supercapacitors, J. Energy Storage 56 (Part B) (2022) 106133.
[68] J. Jung, J. Ryeol Jeong, C. Dang Van, K. Kang, M. Hyung Lee, Laser-assisted patterning of Co–Ni alloy/reduced graphene oxide composite for enhanced micro-supercapacitor performance, ACS Appl. Electron. Mater. 4 (10) (2022) 4840–4848.
[69] S. De, S. Acharya, S. Sahoo, N. Ganesh Chandra, Current trends in MXene research: properties and applications, Mater. Chem. Front. 5 (19) (2021) 7134–7169.
[70] Q. Gao, X. Wang, D.W. Schubert, X. Liu, Review on polymer/MXene composites for electromagnetic interference shielding applications, Advan. Nanocomp. 1 (1) (2024) 52–76.
[71] X. Zheng, H. Zhang, Z. Liu, R. Jiang, X. Zhou, Functional composite electromagnetic shielding materials for aerospace, electronics and wearable fields", Mater. Today Commun. 33 (2022) 104498.
[72] T.A. Oyehan, B. Abiodun Salami, A.A. Abdulrasheed, H.U. Hambali, A. Gbadamosi, E. Valsami-Jones, T.A. Saleh, MXenes: synthesis, properties, and applications for sustainable energy and environment, Appl. Mater. Today 35 (2023) 101993.
[73] Md I. Haque Protyai, A.B. Rashid, A comprehensive overview of recent progress in MXene-based polymer composites: Their fabrication processes, advanced applications, and prospects, Heliyon 10 (17) (2024) 37030.
[74] B. Anasori, M.R. Lukatskaya, Y. Gogotsi, 2D metal carbides and nitrides (MXenes) for energy storage, Nat. Rev. Mater. 2 (2017) 16098. Cao et al., 2019; Chaudhuri and Yun, no date.
[75] A. Sikdar, P. Dutta, S.K. Deb, A. Majumdar, N. Padma, S. Ghosh, U.N. Maiti, Spontaneous three-dimensional self-assembly of MXene and graphene for impressive energy and rate performance pseudocapacitors, Electrochim. Acta 391 (2021) 138959.
[76] A. Gebrekrstos, T. S. Muzata, A. Elias, S. Sinha Ray, Tailoring the properties of 2D nanomaterial-polymer composites for electromagnetic interference shielding and energy storage by 3D printing—a review, Adv. Eng. Mater. 27 (7) (December, 2024) 2402179.
[77] H. Chang, P. Gao, H. Hao, J. Qu, J. Xu, Ma, Hierarchically porous MXene/carbon nanotube/epoxy composites for effective electromagnetic interference shielding and flame retardancy, ACS Appl. Nano Mater. 7 (3) (Feb. 2024) 3168–3178.
[78] X.X. Jin, J.F. Wang, L.Z. Dai, X.Y. Liu, L. Li, Y.Y. Yang, Y.X. Cao, W.J. Wang, H. Wu, S.Y. Guo, Flame-retardant poly(vinyl alcohol)/MXene multilayered films with outstanding electromagnetic interference shielding and thermal conductive performances, Chem. Eng. J. 380 (2020) 122457.
[79] Q.T. Zhou, P.H. Li, Y.Z. Xu, J.M. Feng, C.T. Ma, C.Y. Liu, Shen, An asymmetric sandwich structural cellulose-based film with self-supported MXene and AgNW layers for flexible electromagnetic interference shielding and thermal management, Nanoscale 13 (2021) 2378–2388.
[80] S.D. Lawaniya, S. Kumar, Y. Yu, R. Horst-Günter, Y. Kumar Mishra, K. Awasthi, Functional nanomaterials in flexible gas sensors: recent progress and future prospects, Mater. Today Chem. 29 (2023) 101428.
[81] R. Kumar, N. Goel, M. Hojamberdiev, M. Kumar, Transition metal dichalcogenides-based flexible gas sensors, Sensor Actuat. Phys. 303 (2020) 111875.
[82] D. Burman, A. Sharma, P.K. Guha, Flexible large MoS_2 film based Ammonia sensor, IEEE Sensors Lett. 2 (2) (2018).
[83] R. Kumar, N. Goel, M. Kumar, High performance NO_2 sensor using MoS_2 nanowires network, Appl. Phys. Lett. 112 (2018) 53502,.

[84] S. Sharma, S. Reddy Parne, S.S. Sripada Panda, S. Gandi, Progress in microwave absorbing materials: a critical review, Adv. Colloid Interface Sci. 327 (2024) 103143.
[85] M. Qin, L. Zhang, H. Wu, Dielectric loss mechanism in electromagnetic wave absorbing materials, Adv. Sci. 9 (10) (April 2022) e2105553.
[86] D. Meroni, C. Cionti, L. Silvestrini, N. Gal, M. Cazzaniga, M. Ceotto, G. Buccella, L. Lo Presti, G. Cappelletti, Oxygen vacancies in the spotlight: on the engineering of intrinsic defects in highly defective TiO_2 photocatalysts, J. Photochem. Photobiol. Chem. 444 (2023) 114916.
[87] R. Hazarika, B. Kalita, Effect of oxygen vacancy defects on electronic and optical properties of MgO monolayers: first principles study, Mater. Sci. Eng., B 286 (2022) 115974.
[88] B. Wen, C. Mao-Sheng, H. Zhi-Ling, S. Wei-Li, Z. Lu, L. Ming-Ming, J. Hai-Bo, F. Xiao-Yong, W. Wen-Zhong, J. Yuan, Temperature dependent microwave attenuation behavior for carbon-nanotube/silica composites, Carbon 65 (2013) 124–139.
[89] F. Zhang, N. Li, S. Jun-Feng, L. Xu, J. Li-Chuan, W. Yue-Yi, Y. Ding-Xiang, Recent progress on carbon-based microwave absorption materials for multifunctional applications: a review, Compos. B Eng. 283 (2024) 111646.
[90] Y. Wu, et al., Ultralight graphene foam/conductive polymer composites for exceptional electromagnetic interference shielding, ACS Appl. Mater. Interfaces 9 (10) (2017) 9059–9069.
[91] A.K. Katiyar, A. Tuan Hoang, D. Xu, J. Hong, B. Jin Kim, S. Ji, J.-H. Ahn, 2D materials in flexible electronics: recent advances and future Prospectives, Chem. Rev. 124 (2024) 318–419. Chaudhuri and Yun, no date.
[92] X. Bai, Y. Zhai, Y. Zhang, Green approach to prepare graphene-based composites with high microwave absorption capacity, J. Phys. Chem. C 115 (23) (2011) 11673–11677.
[93] V.K. Singh, A. Shukla, M.K. Patra, L. Saini, R.K. Jani, S.R. Vadera, N. Kumar, Microwave absorbing properties of a thermally reduced graphene oxide/nitrile butadiene rubber composite, Carbon 50 (6) (2012) 2202–2208.
[94] W. Feng, Y. Zhou, H. Xing, et al., Hydrothermal synthesis of nitrogen-doped graphene as lightweight and high-efficient electromagnetic wave absorbers, J. Mater. Sci. Mater. Electron. 32 (2021) 26116–26125.
[95] X. Zhao, Z. Zhang, L. Wang, et al., Excellent microwave absorption property of Graphene-coated Fe nanocomposites, Sci. Rep. 3 (2013) 3421.
[96] X.J. Zhang, G.S. Wang, W.Q. Cao, Y.Z. Wei, J.F. Liang, L. Guo, M.S. Cao, Enhanced microwave absorption property of reduced graphene oxide (RGO)-$MnFe_2O_4$ nanocomposites and polyvinylidene fluoride, ACS Appl. Mater. Interfaces 6 (10) (2014) 7471–7478.
[97] D.N. Ampong, E. Agyekum, F.O. Agyemang, et al., MXene: fundamentals to applications in electrochemical energy storage, Discover Nano 18 (2023) 3.
[98] Y. Qing, et al., Titanium carbide (MXene) nanosheets as promising microwave absorbers, Ceram. Int. 42 (14) (2016) 16412–16416.
[99] W. Feng, et al., Ni-modified Ti3C2 MXene with enhanced microwave absorbing ability, Mater. Chem. Front. 2 (12) (2018) 2320–2326.
[100] J. Liu, et al., Multifunctional, superelastic, and lightweight MXene/polyimide aerogels, Small 14 (45) (2018) 1802479.
[101] Z. Liu, et al., Fabrication of folded MXene/MoS2 composite microspheres with optimal composition and their microwave absorbing properties, J. Colloid Interface Sci. 607 (2022) 633–644.

[102] L. Feng, et al., Two-dimensional transition metal dichalcogenides based composites for microwave absorption applications: a review, J. Phys. Energy 5 (2022) 012001.
[103] X. Liang, X. Zhang, W. Liu, D. Tang, B. Zhang, G. Ji, A simple hydrothermal process to grow MoS_2 nanosheets with excellent dielectric loss and microwave absorption performance, J. Mater. Chem. C 4 (2016) 6816–6821.
[104] L. Xing, X. Li, Z. Wu, X. Yu, J. Liu, L. Wang, C. Cai, W. You, G. Chen, J. Ding, R. Che, 3D hierarchical local heterojunction of MoS_2/FeS_2 for enhanced microwave absorption, Chem. Eng. J. 379 (2020) 122241.
[105] X.-J. Zhang, S.-W. Wang, G.-S. Wang, Z. Li, A.-P. Guo, J.-Q. Zhu, et al., Facile synthesis of NiS_2@MoS_2 core–shell nanospheres for effective enhancement in microwave absorption, RSC Adv. 7 (2017) 22454–22460.
[106] C. Wu, G. Zhao, X. Yu, C. Liu, P. Lyu, G. Maurin, S. Le, K. Sun, N. Zhang, MoS_2/graphene heterostructure with facilitated Mg-diffusion kinetics for high-performance rechargeable magnesium batteries, Chem. Eng. J. 412 (2021) 128736.
[107] N. Li, G.-W. Huang, Y.-Q. Li, H.-M. Xiao, Q.-P. Feng, N. Hu, S.-Y. Fu, Enhanced microwave absorption performance of coated carbon nanotubes by optimizing the Fe_3O_4 nanocoating structure, ACS Appl. Mater. Interfaces 9 (3) (2017) 2973–2983.
[108] J. Li, Y. Xie, L. Weibang, C. Tsu-Wei, Flexible electromagnetic wave absorbing composite based on 3D rGO-CNT-Fe_3O_4 ternary films, Carbon 129 (2018) 76–84.
[109] M.G. Rasul, A. Kiziltas, B. Arfaei, et al., "2D boron nitride nanosheets for polymer composite materials", Npj 2D Mater. Appl. 5 (2021) 56.
[110] M. Wu, Y. Zhou, H. Zhang, W. Liao, 2D boron nitride nanosheets for smart thermal management and advanced dielectrics", Adv. Mater. Interfac. 9 (25) (2022) 2200610.

Further reading

[1] F. Hui, H.A. Bechtel, E. Plis, M.C. Martin, S. Krishna, E. Yablonovitch, A. Javey, Quantum of optical absorption in two-dimensional semiconductors, Proc. Natl. Acad. Sci. 110 (29) (2013) 11688–11691.
[2] M.S. Cao, X.X. Wang, M. Zhang, J.C. Shu, W.Q. Cao, H.J. Yang, X.Y. Fang, J. Yuan, Electromagnetic response and energy conversion for functions and devices in low-dimensional materials, Adv. Funct. Mater. 29 (25) (2019), https://doi.org/10.1002/adfm.201807398.
[3] H. Chaudhuri, Y.-S. Yun, A critical review on the properties and energy storage applications of graphene oxide/layered double hydroxides and graphene oxide/MXenes, J. Power Sourc. 564 (2023). https://doi.org/10.1016/j.jpowsour.2023.232870.